A Study on the Lifetime of Q2L-MMC-DAB's Switches for Wind Turbine Applications

2020 Fifteenth International Conference on Ecological Vehicles and Renewable Energies (EVER)

A Study on the Lifetime of Q2L-MMC-DAB's Switches for Wind Turbine Applications

Babak Khanzadeh, Chengjun Tang, and Torbjörn Thiringer
Department of Electrical Engineering, Chalmers University of Technology, Göteborg, Sweden
Email: ababak@chalmers.se, chengjun.tang@chalmers.se, and torbjorn.thiringer@chalmers.se

***Abstract*—This paper studies the lifetime of semiconductor switches of a dual-active-bridge (DAB) DC-DC converter for wind turbine applications. Quasi-two-level operating modular multilevel converters (MMC) are used as the building blocks of the DAB converter. One of the established lifetime models is used for the lifetime estimation of the switches. Measurement data of an on-shore wind turbine for three hundred days is used as the mission profile. It is shown that the short-term thermal cycles (cycles with frequency in the range of switching frequency) are detrimental to the lifetime estimation of the auxiliary switches of the MMCs' submodules. Thus, neglecting the short-term thermal cycles will overestimate the lifetime of the auxiliary switches by several orders of magnitude. On the other hand, these cycles will not affect the lifetime of the bypass switches considerably. It is also shown that the thermal stress on the secondary-side auxiliary switches is more severe than the primary-side ones. It is suggested that two parallel devices should be used for the secondary-side auxiliary switches; as a consequence, a reasonable lifetime is achieved for the secondary-side auxiliary switches.**

Keywords*—DC-DC power conversion; modular multilevel converter (MMC); three-phase dual-active-bridge (DAB); thermal stress; reliability.

I. Introduction

It has been shown that the generated electrical power from offshore wind parks located far away from the shore can be collected with lower costs if MVDC collection grids are used instead of the existing MVAC collection grids [1]. High-power DC-DC converters are required to realize the MVDC collection grid. They boost up the low voltage output of wind turbines to the medium voltage level of the MVDC grid. Moreover, galvanically isolated DC-DC converters are favored over non-isolated ones due to the high step-up ratio between the two grids for this application [2].

The dual-active-bridge (DAB) configuration, proposed in [3], is a suitable candidate for this application, since its intermediate transformer provides galvanic isolation between the primary and the secondary sides. Modular multilevel converters (MMC) can be used as the building blocks of the DAB, to enable the possibility of achieving medium voltage levels by stacking the low voltage submodules. Moreover, quasi-two-level (Q2L) modulation of the MMCs will provide the possibility to increase the power density by reducing the size of the passive components [4].

The semiconductor switching devices (MOSFET or IGBT) are some of the key components inside the converters. When designing the power devices for converters, reliability is one of the main concerns, since it is intuitive to have a device which can be operated for a long time [5]. Another detrimental factor to the device lifetime is the cyclic peak-to-peak ripple in the device's junction temperature, which is related to the mission profile. Therefore, a lifetime analysis of the converter's switches by considering the mission profile is needed [6].

One of the benefits of the Q2L-modulation of the MMC is the possibility of using smaller devices for the auxiliary switches—the switches that insert the submodules' capacitors in the current flow path—compared to the bypass switches due to the short conduction period and lower peak currents of the auxiliary switches [7]. The design of the submodules and the operation of the Q2L-operating MMC-DAB is investigated in detail in [4], [8]. However, the thermal stresses on switches under this operation are not studied. This paper is intended to fill this gap by providing insight over the thermal cycles of switching devices for the converter mentioned above under the Q2L-modulation. The converter is intended for wind turbine applications, and measurement data from a wind turbine is used as a mission profile for lifetime studies. The converter is modeled in MATLAB using SiC MOSFETs from Cree due to their low switching losses. The junction temperature profiles of switches and respective estimated lifetimes are provided in the forthcoming sections.

978-1-7281-5641-5/20/$31.00

II. Converter Configuration

The configuration of a three-phase DAB converter is shown in Fig. 1(a). Two inverters are connected in a front-to-front structure with a three-phase medium-frequency-transformer (MFT). Each of the two bridges generates periodic waveforms on their three-phase terminals. The active power can be transmitted from one side to another if there is a phase shift between the waveforms of the two bridges [3]. In this paper, the modular multi-level converter (MMC)—shown in Fig. 1(b)—is used as a building block of the DAB converter. Each arm of the MMC is formed by a series connection of half-bridge submodules. The switches inserting the capacitors in the current path are denoted as auxiliary switches, and the rest are referred to as bypass switches as they bypass the submodules.

The converters are modulated with quasi-two-level (Q2L) modulation technique [4], [8]. Fig. 2 illustrates the phase-to-ground voltage waveform of the converter shown in Fig. 1(b), which operates with Q2L modulation and has six submodules per arm. At $\omega t = \theta_2$, all of the submodules of the upper arm in phase-A's leg are bypassed, and the AC terminal is clamped to the positive DC rail. Between $\omega t = \theta_2$ and $\omega t = \theta_4$, a transition from the positive DC rail to the negative DC rail happens. The submodules of the upper arm are inserted one-by-one while the submodules of the lower arm are bypassed sequentially. During the transition time, $T_{\text{transition}}$, the upper and the lower arms share the phase current among themselves. This modulation is called complementary switching [4], [8].

III. Mission Profile and Lifetime Model

A. Mission profile

Since the converter is intended for wind turbine applications, a wind turbine mission profile is required for this study. Wind speed and generated electrical power measurements for 300 days were available for a 2 MW onshore wind turbine. The turbine is located in Munkagård area nearby Tvååker community in Sweden [9]. Fig. 3 shows the measured wind speed and generated electrical power from the turbine mentioned above for 300 days with the measurement frequency of 1 Hz.

B. Lifetime model

The two major failure mechanisms inside the power devices are bond wire degradation and solder fatigue. According to the study in [10], the thermal cycling stresses which in the range of seconds are mainly responsible for the former failure mechanism; while the slow thermal

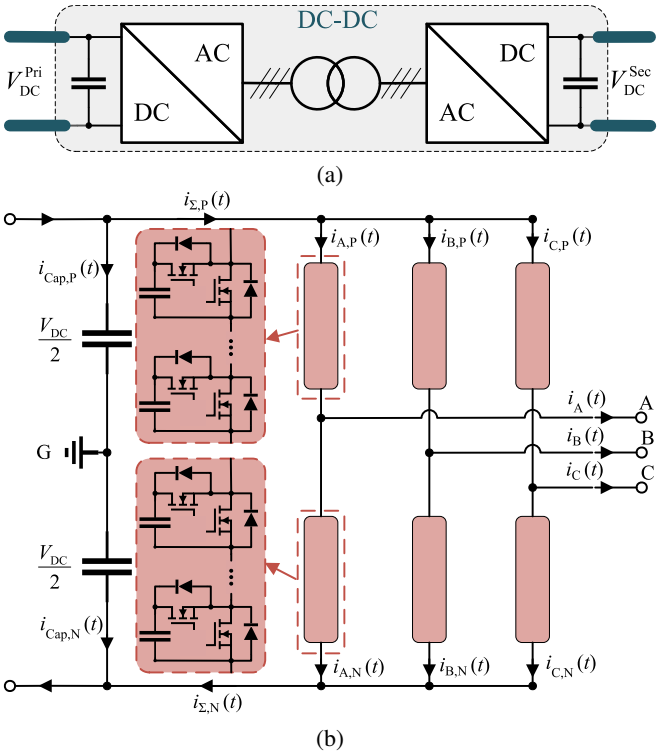

Fig. 1. Topology of the converter. (a) The three-phase DAB DC-DC converter. (b) The modular multi-level converter (MMC) building-block.

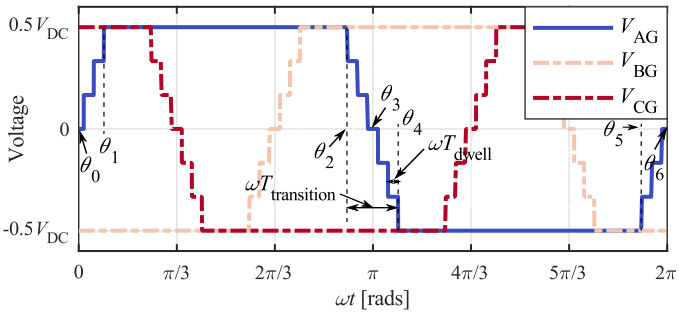

Fig. 2. Phase-to-ground waveforms of the Q2L-MMC-DAB converter.

cycling stresses caused by ambient temperature variations are more related to the latter one. For this study, measurement data for the temperature inside nacelle was not available. Therefore, for the simplicity of analysis, the heat sink temperature is set as a fixed value, which means the slow thermal cycling stresses are neglected. In that sense, the bond wire degradation is the main factor to be considered when conducting the lifetime analysis in this work.

Different lifetime models for silicon-based power devices have been summarized in [11]. For the SiC MOSFETs, the research on the lifetime models is still ongoing [12]. However, if the bond wire degradation is the only factor which needs to be investigated, some experience from previous works can still provide a rea-

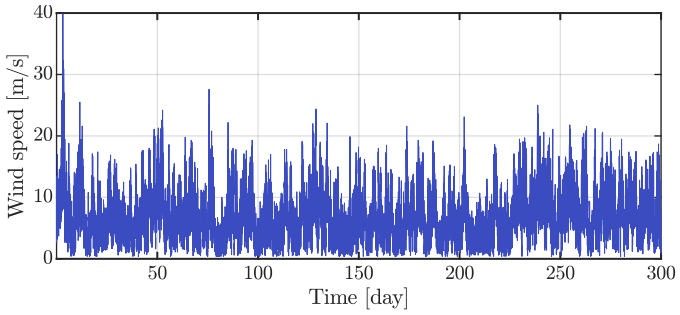

(a)

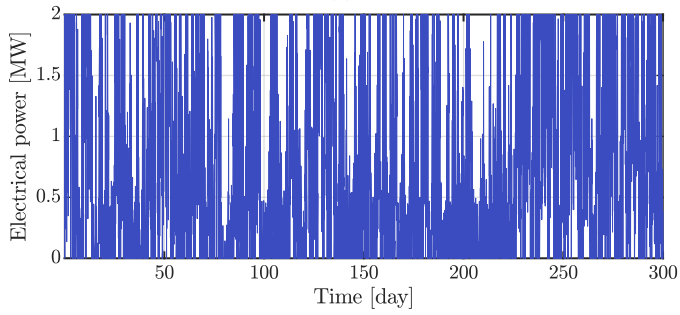

(b)

Fig. 3. Three hundred days mission profile of a wind turbine with one Hertz measurement frequency. (a) For the wind speed. (b) For the generated electrical power.

sonable estimation of the lifetime. Therefore, a lifetime model which seperates the effect of solder fatigue in [13] is used to calculate the life cycles, N_f, of the switches with respect to the temperature swing, ΔT_j, and the medium junction temperature, T_jm,

$$N_f = A \times (\Delta T_\mathrm{j})^{\alpha} \times (ar)^{\beta_1 \Delta T_\mathrm{j} + \beta_0} \times [\frac{C + (t_\mathrm{on})^{\gamma}}{C+1}] \times \exp(\frac{E_a}{k_b \times T_\mathrm{jm}}) \times f_\mathrm{diode} \quad (1)$$

where the parameters are given in Table I. The parameter of the load pulse duration t_on which used in this study is different from the value in [13]. For the thermal cycles which are longer than one second, t_on is selected as $1\,\mathrm{s}$; while for the thermal cycles shorter than one second, t_on is selected as $0.07\,\mathrm{s}$.

TABLE I. LIFETIME MODEL PARAMETERS

Parameter	Value	Parameter	Value
A	3.4368×10^{14}	α	-4.923
β_1	-9.012×10^{-3} 1/K	ar	0.31
β_0	1.942	C	1.434
E_a	6.606×10^{-2} eV	γ	-1.208
k_b	8.62×10^{-5} eV/K	f_diode	1

The accumulated damage D of the switch under a single run of this mission profile can be determined by Miner's rule [14],

$$D = \sum_{i=1}^{n} \frac{N_i}{N_{fi}} \quad (2)$$

where N_i can be determined from the Rainflow counting algorithm and N_{fi} can be calculated from (1). The inverse of D is the repetition rate, N_r, for the considered mission profile. For example, if N_r equals to 1, then the switch can only withstand a single run of the considered mission profile, which is 300 days.

IV. Simulation and Analysis

A. Case Setup

The converter's model is implemented in MATLAB. The converter is rated for 2 MW. For simplicity, it is assumed that the primary and the secondary side DC links have the same voltage ratings. The converter is switched with 5 kHz as a further higher switching frequency might not be beneficial for improving the power density [15]. The transition time is assumed to be constant and equal to 5% of the fundamental period for all power levels. Since the objective is not a study on the transformer, the MFT is modeled as a leakage inductance to only form the required waveforms of the DC-DC converter. The value of the leakage inductance is determined using the method explained in [16]. Table II depicts the specifications of the converter under simulation.

TABLE II. SIMULATED DC-DC CONVERTERS' SPECIFICATIONS

Parameter	Value	Parameter	Value
$V_\mathrm{DC,nom}^\mathrm{Pri}$	5 kV	P_nom	2 MW
$V_\mathrm{DC,nom}^\mathrm{Sec}$	5 kV	f_sw	5 kHz
V_sw	1.7 kV	$T_\mathrm{transition}$	10 μs
N_SM	5	L_leakage	92 μH

1.7 kV SiC MOSFETs, namely CAS300M17BM2 and C2M0045170P are used for this study [17], [18]. The datasheet is used to calculate the conduction and the switching losses based on the junction temperature and the operational electrical parameters. The switches' thermal behavior is modeled using a fourth-order Foster network representing the junction-to-case thermal impedance. As measurement data were not available for the inside temperature of the nacelle, it is assumed that the case temperatures of the switches are constant at $40\,^\circ\mathrm{C}$.

Direct simulation of a converter switching with $5\,\mathrm{kHz}$ for 300 days of mission profile is not feasible. Therefore, the study is divided into two parts; the first to calculate the life consumption for long-term thermal cycles (i.e. longer than one second) and the second to perform the calculations for short-term thermal cycles (i.e. shorter than one second). The converter is simulated for full-load and partial loads and the steady-state junction temperatures are stored. CAS300M17BM2 and C2M0045170P

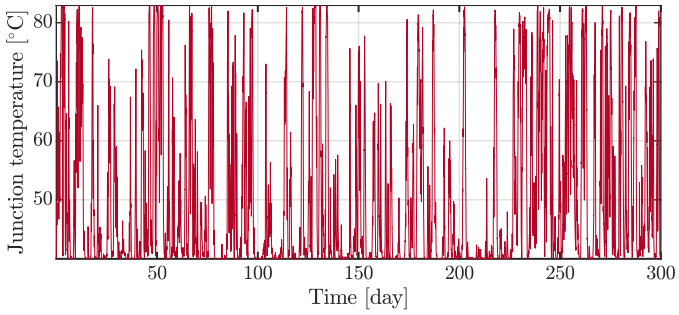

Fig. 4. Low-pass-filtered junction temperature profile for one of the primary-side bypass switches.

MOSFETs are used as bypass and auxiliary switches, respectively, of both the primary and the secondary inverters. The average junction temperature profile of the switches are obtained by combining the converter's power profile—shown in Fig. 3(b)—and the average junction temperatures of the switches obtained from the simulations. Fig. 4 shows the low-pass-filtered average junction temperature profile for one of the primary-side bypass switches.

The Rainflow counting algorithm is employed to identify the number of thermal cycles in the junction temperature profile. In addition to the cycle numbers, the temperature swing ΔT_j and the medium junction temperature T_jm of the corresponding cycles are extracted as well. Fig. 5 shows the Rainflow counting results for one of the bypass switches of the secondary-side. N_{fi} of each switch is calculated by inputting ΔT_j and T_jm from the Rainflow counting into (1). Then the lifetime of the switches is estimated by using (2) and the length of the mission profile.

TABLE III. LIFETIME OF SWITCHES

Lifetime [years]	**Bypass switches**				
	#1	**#2**	**#3**	**#4**	**#5**
Primary side	552	552	552	552	550
Secondary side	2.7e+5	2.5e+5	2.7e+5	2.6e+5	2.5e+5
Lifetime [years]	**Auxiliary switches**				
	#1	**#2**	**#3**	**#4**	**#5**
Primary side	1.3e+8	2.3e+8	1.4e+8	2.1e+8	1.1e+8
Secondary side	5.1e+4	5.9e+4	4.9e+4	4.4e+4	4.6e+4

B. Analysis of Results

Table III summarizes the lifetimes of the switches for one of the inverter's arms. Since complementary switching is used and the intermediate three-phase system is assumed to be symmetrical, the same lifetimes will be achieved for the corresponding switches of the other arms of the primary and the secondary side inverters. As can be seen, there is a variation in the lifetime of the switches in different submodules of the inverter. The reason is the sorting algorithm; the submodules are sorted every

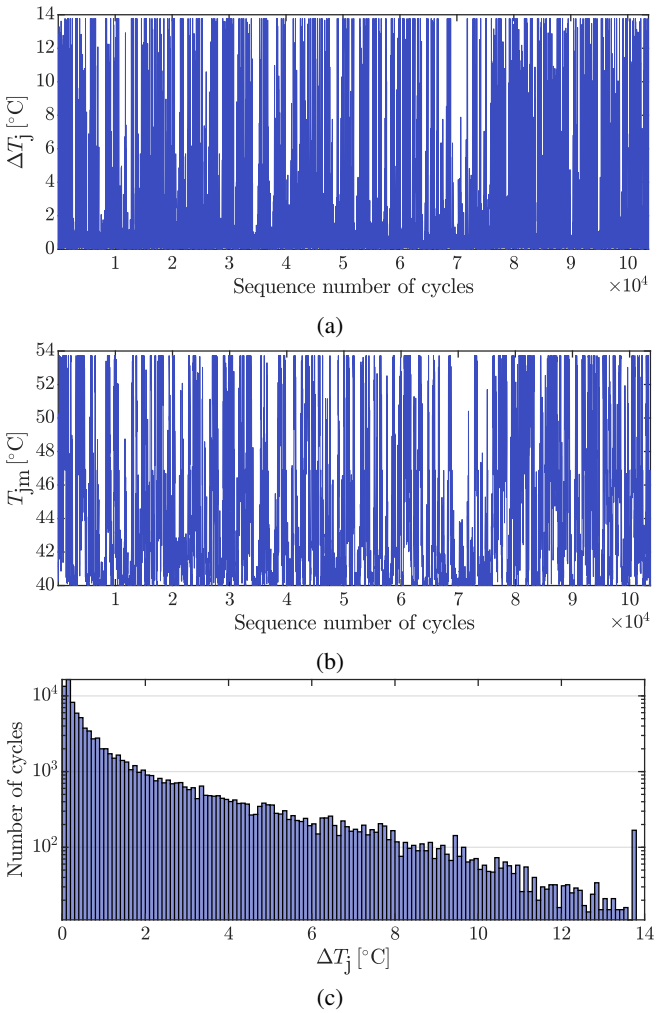

Fig. 5. Rainflow counting results for one of the secondary-side bypass switches. (a) ΔT_j with respect to the cycle number. (b) T_jm with respect to the cycle number. (c) Histogram distribution of cycles with respect to ΔT_j.

half-cycle based on their voltages and the direction of the phase currents—irrespective of the junction temperatures. This causes a slight variation between the junction temperatures of the switches of the submodules and therefore affecting their lifetime. Another observation is the long lifetime of the switches. This is due to the small ΔT_j and the low average temperature of the switches, as shown in Fig. 5.

Considering only the long-term thermal cycles might not be sufficient to assess the stress on the switches for this converter topology. Fig. 6 depicts the junction temperature profiles of one of the submodules of the primary-side and the secondary-side inverters for the full-load operation and 30 fundamental cycles. The bypass switches are conducting the currents for almost half a cycle and have moderate temperature swings of $2.6\,^{\circ}\mathrm{C}$ and $0.8\,^{\circ}\mathrm{C}$ for the primary and the secondary sides respectively. However, the auxiliary switches conduct high currents for a fraction of the fundamental cycle,

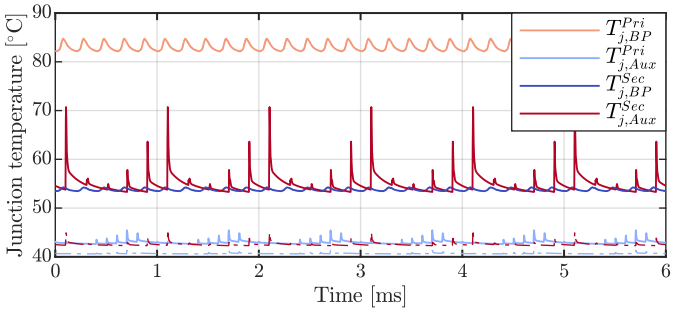

Fig. 6. Junction temperatures of inverters' first submodule's switches' at the full-load. The dashed line is the Junction temperatures with two C2M0045170P in parallel as the auxiliary switches.

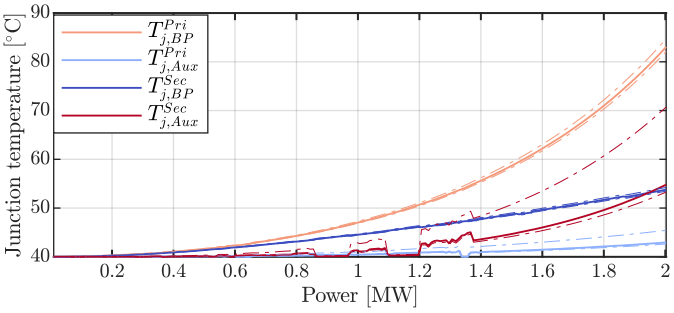

Fig. 7. Junction temperatures of inverters' first submodule's switches. The solid lines are the average junction temperatures, and the dashed lines are the bounds of the temperature profiles.

which results in severe temperature swings of 2.5 °C and 17 °C for the primary and the secondary side inverters respectively.

For the majority of the conduction period, the primary-side bypass switches and the secondary-side auxiliary switches conduct positive currents and operate in the forward conduction mode. On the other hand, the secondary-side bypass switches and the primary-side auxiliary switches conduct negative currents, and therefore, the MOSFETs are operating in the third-quadrant. The conduction losses predominate in MOSFETs, and the operation in third-quadrant results in lower conduction losses. Therefore, the primary-side auxiliary switches and the secondary-side bypass switches—which operate in the third-quadrant—are less thermally stressed compared to their counterparts in the other inverter, as shown in Fig. 6.

Fig. 7 shows the junction temperatures of one of the submodules' switches as a function of the power transmitted by the converter. The solid lines are the average junction temperatures, and the dashed lines depict the maximum and the minimum temperatures of the switch. As can be seen, the secondary-side auxiliary MOSFET is the most thermally stressed switch in both full-load and partial loads, therefore, expected to have a shorter lifetime compared to other switches. To consider these short-term temperature oscillations, the power profile—shown in Fig. 3(b)—is binned into 200 power intervals. Fig. 8 shows the duration of the power production from the turbine for each power interval. The mean value of the power in each bin is considered as the representative of that bin, and the temperature profile for the representative power level is used to calculate the life consumption of the switches.

The total life consumption of a switch can be calculated by summing up the life consumption from the long-term and the short-term thermal cycles. As the same mission profile is used to calculate both of the life

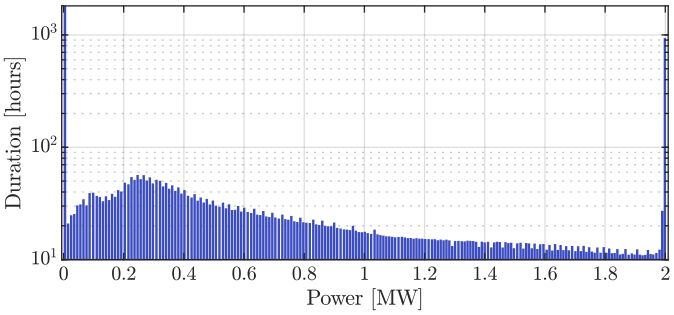

Fig. 8. The power distribution of the wind profile given in Fig. 3.

consumptions, the lifetime can be easily calculated by dividing the length of the mission profile by the total life consumption. Fig. 9 shows the lifetime of the primary-side and the secondary-side inverters' first submodule's switches. The thinner bars are the lifetimes considering the short-term temperature cycles, and the thick bars are without them. As can be seen, neglecting the short-term cycles has a negligible effect on the lifetime of the bypass switches. The reason is that the temperature variations are insignificant for the bypass switches, as shown in Fig. 7. However, there is a drastic decrease in the lifetime of auxiliary switches when the short-term cycles are considered—especially for the secondary side inverter.

The secondary side submodules will reach the end of their life in less than a year—as shown in Fig. 9—if C2M0045170P is used as the auxiliary switches. Two C2M0045170P in parallel are used instead to solve this issue. As can be seen, the lifetime of the secondary side auxiliary switches can be extended considerably by this change. Even though the lifetime of the primary-side auxiliary switches can also be extended with the same approach, it will increase the cost of the primary-side auxiliary switches by a factor of two. Any which way, the bypass switch will be the detrimental factor for the lifetime of the submodule of the primary-side inverter. It is noteworthy to mention that the application of the

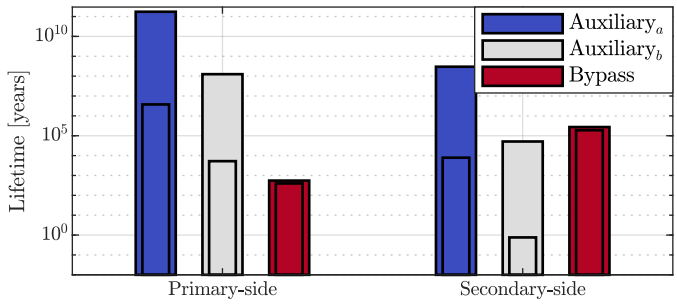

Fig. 9. Lifetime comparison of the primary-side and the secondary-side inverters' first submodule's switches (The lifetime considering the short-term thermal cycles are illustrated with the thinner bars) where $\{a, b\} \in \{2 \times \text{C2M0045170P},\ \text{C2M0045170P}\}$.

converter in this paper is unidirectional. Therefore, the secondary-side auxiliary switches will always be more stressed compared to the primary-side auxiliary switches.

V. Conclusion

The study of the Q2L-operating MMC-DAB's—with MOSFETs as semiconductor switches—revealed that the primary-side bypass and the secondary-side auxiliary switches have higher average junction temperatures compared to the secondary-side bypass and the primary-side auxiliary switches respectively. Moreover, it is shown that the auxiliary switches are more thermally stressed compared to the bypass switches due to the impulsive conduction of currents. Therefore, it is important to consider the switching frequency thermal cycles for these switches. It is demonstrated that secondary-side auxiliary switches will not be able to endure a single mission profile; While their primary-side counterparts will have an acceptable lifetime. To solve this issue, it is suggested that two parallel switches can be used on the secondary-side converter for the auxiliary switches. It is shown that with this approach, the lifetime of the secondary-side switches can be extended to an acceptable range.

Acknowledgment

This work has received funding from Energimyndigheten under project number P43048-1 and European Union's Horizon 2020 research and innovation program under grant agreement No 764011.

References

[1] D. Valcan, P. C. Kjær, L. Helle, S. Sahukari, M. Haj-Maharsi, and S. Singh, "Cost of energy assessment methodology for offshore ac and dc wind power plants," in *2012 13th International Conference on Optimization of Electrical and Electronic Equipment (OPTIM)*, pp. 919–928, May 2012.

[2] J. D. Páez, D. Frey, J. Maneiro, S. Bacha, and P. Dworakowski, "Overview of dc–dc converters dedicated to hvdc grids," *IEEE Transactions on Power Delivery*, vol. 34, pp. 119–128, Feb 2019.

[3] R. W. A. A. De Doncker, D. M. Divan, and M. H. Kheraluwala, "A three-phase soft-switched high-power-density dc/dc converter for high-power applications," *IEEE Transactions on Industry Applications*, vol. 27, pp. 63–73, Jan 1991.

[4] I. A. Gowaid, G. P. Adam, A. M. Massoud, S. Ahmed, D. Holliday, and B. W. Williams, "Quasi two-level operation of modular multilevel converter for use in a high-power dc transformer with dc fault isolation capability," *IEEE Transactions on Power Electronics*, vol. 30, pp. 108–123, Jan 2015.

[5] M. H. Rashid, *Power electronics handbook*. Butterworth-Heinemann, 2017.

[6] K. Ma, M. Liserre, and F. Blaabjerg, "Lifetime estimation for the power semiconductors considering mission profiles in wind power converter," in *2013 IEEE Energy Conversion Congress and Exposition*, pp. 2962–2971, IEEE, 2013.

[7] I. A. Gowaid, G. P. Adam, A. M. Massoud, S. Ahmed, and B. W. Williams, "Hybrid and modular multilevel converter designs for isolated hvdc–dc converters," *IEEE Journal of Emerging and Selected Topics in Power Electronics*, vol. 6, pp. 188–202, March 2018.

[8] I. A. Gowaid, G. P. Adam, S. Ahmed, D. Holliday, and B. W. Williams, "Analysis and design of a modular multilevel converter with trapezoidal modulation for medium and high voltage dc-dc transformers," *IEEE Transactions on Power Electronics*, vol. 30, pp. 5439–5457, Oct 2015.

[9] T. Thiringer, J. Paixao, and M. Bongiorno, *Monitoring of ride-through ability of a 2MW Wind turbine in Tvåker, Halland*. Elforsk, 2009.

[10] P. D. Reigosa, H. Wang, Y. Yang, and F. Blaabjerg, "Prediction of bond wire fatigue of igbts in a pv inverter under a long-term operation," *IEEE Transactions on Power Electronics*, vol. 31, no. 10, pp. 7171–7182, 2015.

[11] J. Lutz, H. Schlangenotto, U. Scheuermann, and R. De Doncker, *Semiconductor power devices*. Springer, 2 ed., 2018.

[12] B. Hu, J. O. Gonzalez, L. Ran, H. Ren, Z. Zeng, W. Lai, B. Gao, O. Alatise, H. Lu, C. Bailey, *et al.*, "Failure and reliability analysis of a sic power module based on stress comparison to a si device," *IEEE Transactions on Device and Materials Reliability*, vol. 17, no. 4, pp. 727–737, 2017.

[13] U. Scheuermann, R. Schmidt, and P. Newman, "Power cycling testing with different load pulse durations," in *7th IET International Conference on Power Electronics, Machines and Drives (PEMD 2014)*, pp. 1–6, IET, 2014.

[14] M. A. Miner, "Cumulative damage in fatigue," *Journal of Applied Mechanics*, vol. 12, no. 3, p. A159–A164, 1945.

[15] M. A. Bahmani, T. Thiringer, A. Rabiei, and T. Abdulahovic, "Comparative study of a multi-mw high-power density dc transformer with an optimized high-frequency magnetics in all-dc offshore wind farm," *IEEE Transactions on Power Delivery*, vol. 31, pp. 857–866, April 2016.

[16] B. Alikhanzadeh, T. Thiringer, and M. Kharezy, "Optimum leakage inductance determination for a q2l-operating mmc-dab with different transformer winding configurations," in *2019 20th International Symposium on Power Electronics (Ee)*, pp. 1–6, Oct 2019.

[17] "CAS300M17BM2: 1700-V, 8.0-mΩ, Silicon Carbide, Half-Bridge Module." https://www.wolfspeed.com/power/products/sic-power-modules/cas300m17bm2.

[18] "C2M0045170P: Silicon Carbide Power MOSFET C2M Planar MOSFET Technology N-Channel Enhancement Mode." https://www.wolfspeed.com/power/products/sic-mosfets/c2m0045170p.